



1 **The impact of organic nitrates on summer ozone formation in Shanghai,**

2 **China**

3 Chunmeng Li¹, Xiaorui Chen^{2,3*}, Haichao Wang^{2,3}, Tianyu Zhai⁴, Xuefei Ma⁵, Xiping Yang⁴, Shiyi
4 Chen⁵, Min Zhou⁶, Shengrong Lou⁶, Xin Li⁵, Limin Zeng⁵, Keding Lu^{5*}

5 ¹ Center for Environmental Metrology, The National Institute of Metrology, Beijing 100029, China.

6 ² School of Atmospheric Sciences, Sun Yat-sen University, Zhuhai, Guangdong, 519082, China.

7 ³ Guangdong Provincial Observation and Research Station for Climate Environment and Air Quality
8 Change in the Pearl River Estuary, Key Laboratory of Tropical Atmosphere-Ocean System, Ministry
9 of Education, Southern Marine Science and Engineering Guangdong Laboratory (Zhuhai), Zhuhai,
10 519082, China.

11 ⁴ State Environmental Protection Key Laboratory of Vehicle Emission Control and Simulation,
12 Chinese Research Academy of Environmental Sciences, Beijing, 100012, China

13 ⁵ State Key Joint Laboratory of Environmental Simulation and Pollution Control, The State
14 Environmental Protection Key Laboratory of Atmospheric Ozone Pollution Control, College of
15 Environmental Sciences and Engineering, Peking University, Beijing, 100871, China.

16 ⁶ State Environmental Protection Key Laboratory of the Cause and Prevention of Urban Air Pollution
17 Complex, Shanghai Academy of Environmental Sciences, Shanghai, 200233, China.

18

19 * Correspondence: chenxr95@mail.sysu.edu.cn; k.lu@pku.edu.cn

20 **Abstract**

21 Organic nitrates serve as important secondary oxidation products in the atmosphere, playing a crucial
22 role in the atmospheric radical cycles and influencing the production of secondary pollutants (ozone
23 (O₃) and secondary organic aerosols). However, field measurements of organic nitrates are scarce in
24 China, and a comprehensive localized mechanism for organic nitrates is absent, hindering effective
25 pollution mitigation strategies. In this study, we conducted measurements of ambient gaseous organic
26 nitrates and examined their effects on local O₃ production at a polluted urban site in eastern China
27 during summer. The average daytime concentrations of alkyl nitrates (ANs) and peroxy nitrates (PNs)
28 throughout the campaign were 0.5±0.3 ppbv and 0.9±0.7 ppbv, respectively, with peaks reaching up to
29 1.6 ppbv and 3.6 ppbv. An observation-constrained box model, incorporating an updated mechanism
30 for organic nitrates, was employed to assess the environmental impact of these compounds. The model
31 results indicated that PNs production inhibited the daytime O₃ production by 16% (0.8 ppbv/h), which
32 is relatively low compared to previous studies. Furthermore, scenario analyses revealed that production
33 yields (α) of ANs would alter the response of O₃ formation to precursors due to varying compositions
34 of volatile organic compounds. Our results suggest that blind pollution control may cause ineffective
35 pollution prevention and highlight the necessity of a thorough understanding on organic nitrate



36 chemistry for local O₃ control strategy.

37 1. Introduction

38 Tropospheric ozone, as an important oxidant, influences the atmospheric lifetimes of trace gases
39 through its involvement in photochemical processes, thereby playing a crucial role in climate change
40 and atmospheric chemistry. There is a broad consensus that high near-surface ozone concentrations are
41 hazardous to human health and environmental ecosystems, particularly affecting the human respiratory
42 and cardiovascular systems, and result in decreased yields of various crops (Ashmore, 2005; Xue and
43 Zhang, 2023). A scientific assessment of tropospheric ozone is essential for the development of public
44 health policies and for addressing long-term air pollution challenges (Monks et al., 2015). Primary
45 pollutants, such as nitrogen oxides (NO_x) and volatile organic compounds (VOCs), participate in the
46 formation of HO_x radicals (RO_x = RO₂ + HO₂ + OH) cycles and NO_x cycles under sunlight, leading to
47 the continuous production of ozone as a secondary oxidation product within these cycles. In addition
48 to the reaction between OH and NO₂ that produces HNO₃ as part of chain termination reactions, the
49 interaction of RO₂ and NO that produces organic nitrates is of increasing concern (Present et al., 2020).
50 The atmospheric production of organic nitrates consumes both NO_x and RO₂. Therefore, the chemistry
51 of organic nitrates will significantly influence the prevention and control of ozone, with NO_x and VOCs
52 serving as independent variables.

53 Both anthropogenic activities and natural processes contribute to the emissions of NO_x and VOCs,
54 which are produced from RO₂ in the presence of oxidants such as OH. Subsequently, RO₂ reacts with
55 NO to yield NO₂ and RO. After that, NO₂ photolysis produces O₃, while RO is converted into HO₂
56 through an isomerization reaction, thereby forming the ozone production cycle. Within the cycle, a
57 branching reaction between RO₂ and NO leads to the formation of alkyl nitrates (RONO₂, ANs), while
58 RO₂ may also react with NO₂ to generate peroxy nitrates (RO₂NO₂, PNs). Given that PNs are prone to
59 thermal dissociation near the surface (Roberts and Bertman, 1992), they can influence O₃ production
60 by modifying the availability of NO_x and RO_x. Due to the competitive production dynamics between
61 PNs and O₃, numerous field observations and model simulations have been conducted to investigate
62 the impact of peroxyacetyl nitrate (PAN) on O₃ production (Liu et al., 2021; Zeng et al., 2019; Zhang
63 et al., 2020). As another key secondary oxidation product, the branching ratio (α) for ANs formation
64 varies between 0.1% and 35% (Perring et al., 2013). Some values of α , which have not been quantified
65 in the laboratory, are estimated through structure-activity relationships (Arey et al., 2001; Reisen et al.,
66 2005; Teng et al., 2015; Yeh and Ziemann, 2014a; Yeh and Ziemann, 2014b). Multiple field
67 observations revealed a strong linear correlation between ANs and O₃, with a correlation coefficient
68 (r^2) exceeding 0.5, further substantiating the competitive relationship between ANs and O₃ (Aruffo et
69 al., 2014; Day et al., 2003; Flocke et al., 1998).

70 Currently, research on the effects of ANs on O₃ distribution is predominantly located in Europe
71 and the United States. Following the first in situ measurement of total organic nitrates through thermal
72 dissociation laser-induced fluorescence instrument (TD-LIF) by Day et al., field observations of total
73 ANs have been continuously conducted to study the role of ANs in the nitrogen cycle (Aruffo et al.,
74 2014; Browne et al., 2013; Chen et al., 2017; Darer et al., 2011; Day et al., 2003; Sadanaga et al., 2016).
75 In conjunction with field observations and model simulations, Farmer et al. were the first to indicate
76 that ANs influence the sensitivity of NO_x-VOCs-O₃ (Farmer et al., 2011). As NO_x emissions decrease
77 due to pollution control measures, ANs chemistry is expected to play an increasingly significant role



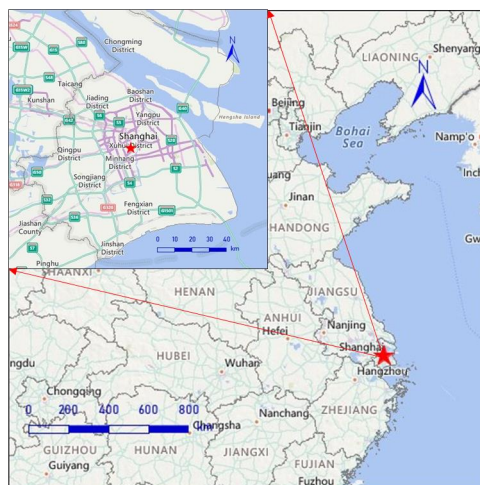
78 in O₃ simulations (Present et al., 2020; Zare et al., 2018). Current mechanisms for O₃ simulations
79 generally achieve reasonable predictions in large-scale models; however, they exhibit deviations
80 exceeding 10 ppbv in regional simulations (Young et al., 2018). Subsequent studies have demonstrated
81 that refining the ANs chemistry can further improve the simulation performance for O₃ (Schwantes et
82 al., 2020). ANs are predominantly produced through oxidation reactions facilitated by OH, O₃, and
83 NO₃. The daytime ANs are mainly contributed by the OH channel, whereas during nighttime, the
84 contribution of the NO₃ channel is linked to significantly increased yields of ANs (Liebmann et al.,
85 2018; Ng et al., 2017; Zare et al., 2018). Presently, the enhancement of ANs chemistry mainly focuses
86 on BVOCs, particularly isoprene and monoterpenes. These researches aim to enhance the yield of ANs
87 derived from BVOCs, the re-release ratio of ANs to NO_x, and the contribution of ANs to aerosols
88 (Fisher et al., 2016; Romer et al., 2016; Travis et al., 2016; Zare et al., 2018). Despite the establishment
89 of a complete mechanism scheme at present, significant uncertainties remain in ANs simulation, which
90 may introduce substantial uncertainties into the O₃ simulation.

91 Atmospheric pollution is common across China, particularly in the Yangtze River Delta. Shanghai,
92 as a highly urbanized metropolis in the Yangtze River Delta, has rendered the region's complex
93 pollution due to its rapid economic growth and urbanization (Wang et al., 2022; Zhu et al., 2021).
94 Previous studies have shown a significant increase in near-surface O₃ levels from 2006 to 2016 in
95 Shanghai (Gao et al., 2017). However, research on the ANs chemistry and their impact on O₃ pollution
96 remains limited in this area. In addition, most field measurements of ANs have focused on short-chain
97 species (Ling et al., 2016; Song et al., 2018; Sun et al., 2018; Wang et al., 2013), which have been
98 observed to exert a typical inhibition effect on daytime O₃ production. A limited number of total ANs
99 measurements found that both ANs and O₃ production were in the VOC-limited regime (Li et al., 2023).
100 To further investigate the influence of organic nitrates on O₃ production, this study describes the
101 distribution of organic nitrates based on a comprehensive field campaign conducted in Shanghai,
102 analyzes the effects of organic nitrates on O₃ production through model simulations, and offers
103 recommendations for the prevention and control of ozone pollution in the region.

104 **2. Methodology**

105 **2.1 Measurement site and instrumentations**

106 A comprehensive campaign was conducted in Shanghai to further investigate the chemical
107 behavior of organic nitrates in urban environments across China. As depicted in Fig. 1, the site is
108 located in the Xuhui District of Shanghai (121.44°E, 31.18°N), in proximity to the Shanghai Inner
109 Ring Viaduct, surrounded by numerous residential and office areas without significant industrial
110 emission sources. The site is mainly influenced by morning-evening rush hours, as well as the transport
111 of air masses to the urban location. The overall wind speed was low, predominantly originating from
112 the east. All the measurement instruments were housed in the temperature-controlled room within the
113 laboratory building at the Shanghai Academy of Environmental Sciences. Thermal Dissociation-
114 Cavity Enhanced Absorption Spectroscopy (TD-CEAS) was positioned on the 7th floor about 25 m
115 above ground level, with the sampling tube extending out through the window.



116

117 **Figure 1.** Map of the city of Shanghai and the surrounding area (@ MeteoInfoMap). The red star is the location of
 118 the campaign site.

119 The Shanghai campaign focused on studying summer ozone pollution, with the chemical
 120 parameters presented in Table 1. Organic nitrates were measured by TD-CEAS with a sampling flow
 121 rate of 3 L/min and a sampling duration of 3 min for alternating measurements of NO₂, PNs, and ANs.
 122 The sampling apparatus consisted of a 2-meter-long 1/4-inch tetrafluoroethylene (TFE) tube, through
 123 which the atmosphere was filtered through a TFE particulate filter. The membrane was replaced once
 124 a day to mitigate the interference caused by wall loss. The measurement of PAN was conducted by gas
 125 chromatography electron capture detection (GC-ECD). The Measurement of N₂O₅ was performed via
 126 CEAS, which relies on the thermal dissociation of N₂O₅ to yield NO₃. Particulate nitrates and gaseous
 127 HNO₃ were measured online by AeRosols and Gases (MARGA), where soluble substances were
 128 quantified through ion chromatography following dissolution. The measurements of HONO were
 129 finished by CEAS during the campaign. Measurements of VOCs were achieved using a combination
 130 of GC-FID and GC-MS, with GC-MS predominating due to the limited species measured by GC-FID.
 131 The photolysis rate constant (J value) was determined using a spectrum radiometer with a time
 132 resolution of 20 s. Additionally, simultaneous measurements of other trace gases such as NO, NO₂,
 133 SO₂, CO, O₃, and PM_{2.5} were conducted using commercial instruments.

134 **Table 1.** Measured species for organic nitrates analysis and instrument time resolution, accuracy, and detection
 135 limitation.

Parameters	Measurement technique	Time resolution	Accuracy	Detection limit
ANs, PNs, NO ₂	TD-CEAS	3 min	± 8%	93 pptv
PAN	GC-ECD	5 min	± 10%	5 pptv
N ₂ O ₅	CEAS	1 min	± 19%	2.7 pptv
NO	Thermo 42i	1 min	± 10%	60 pptv
NO ₂	Chemiluminescence	1 min	± 10%	300 pptv
HONO	CEAS	1 min	± 3%	100 pptv



Particulate nitrate	2060 MARGA	1 h	± 3%	0.01 $\mu\text{g}/\text{m}^3$
HNO ₃	2060 MARGA	1 h	± 3%	0.01 $\mu\text{g}/\text{m}^3$
SO ₂	Thermo 43i-TLE	1 min	± 16%	50 pptv
HCHO	Hantzsch fluorimetry	1 min	± 5%	25 pptv
CO	Thermo 48i-TLE	1 min	± 16%	50 pptv
O ₃	Thermo 49i	1 min	± 5%	0.5 ppbv
PM _{2.5}	Thermo TEOM	1 min	± 5%	0.1 $\mu\text{g}/\text{m}^3$
VOCs	GC-FID/GC-MS	1 h	± 30%	20-300 pptv
J value	Spectrum radiometer	20 s	± 10%	$5 \times 10^{-5} \text{ s}^{-1}$

136

137 2.2 Model calculation

138 To investigate the impact of ANs chemistry on O₃ production, a box model was employed to
139 simulate the photochemistry processes. The mechanism of the model was enhanced based on RACM2
140 (Regional Atmospheric Chemical Mechanism version 2). This box model simulates the
141 physicochemical processes occurring within a defined volume for each reactant. It utilizes measured
142 parameters as the boundary condition to simulate the chemistry process while allowing for convenient
143 adjustments to the mechanism. The model generates files detailing concentration changes, budget
144 processes, and reaction rates, thereby providing an efficient means to simulate ground-level pollutants.
145 In this study, the box model was constrained by various parameters, including J values, O₃, NO, NO₂,
146 CO, HONO, VOCs, RH, temperature, and pressure, with the time step set to 1h. The deposition process
147 was quantified using the deposition rate and the boundary layer height, with the dry deposition rate
148 established at 1.2 cm/s and the boundary layer height constrained by data obtained from NASA.

149 The RACM2 facilitates classification through the distribution of functional groups and
150 subsequently delineates reactions involving 17 stable non-organic compounds, 4 inorganic
151 intermediates, 55 stable organic compounds, and 43 intermediate organic species within the
152 mechanism. However, the mechanism description for ANs is notably abbreviated. The various ANs,
153 characterized by differing functional groups, are treated as a unified entity, thereby neglecting the
154 influence of functional groups on the underlying chemistry. Consequently, this study builds on the
155 previous research and further evaluates the updates of the mechanism (Li et al., 2023). These
156 mechanistic updates are developed based on the work of Zare et al. and primarily encompasses the
157 oxidation processes of BVOCs by OH and NO₃, as well as the deposition and the aerosol uptake, which
158 are detailed in the SI (Zare et al., 2018). Accordingly, three mechanistic schemas are compared based
159 on the campaign, which will be elaborated upon in subsequent sections. A box model based on the
160 above mechanism is used to calculate the ozone production rate (P(O₃)) (Tan et al., 2017b). P(O₃) was
161 quantified based on the net production rate of O_x (the sum of O₃ and NO₂), by subtracting the O_x
162 depletion from the instantaneous O_x production. The simulation uncertainty of the box model is about
163 40%, introduced mainly by the simplified reaction rate constants, photolysis rate constants, and near-
164 ground deposition (Lu et al., 2013).

165 To facilitate the assessment of the impacts of ANs on local O₃ pollution, we further conducted a
166 simplified box model based on the steady-state assumption approach. Several studies have examined
167 the combined effect of α and VOCs reactivity on local O₃ levels using this approach (Farmer et al.,



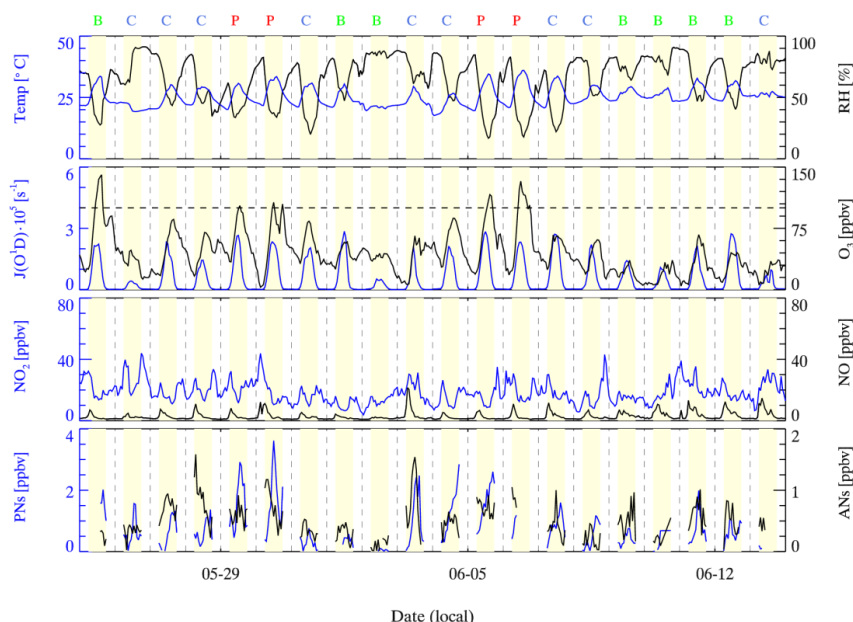
168 2011; Present et al., 2020; Romer et al., 2016; Romer et al., 2018). Briefly, the production pathway of
169 ANs is simplified according to VOCs categories and the production rate of OH and HO₂ (P(HO_x)) is
170 fixed to a constant value. VOCs are categorized into two primary groups: non-oxygenated VOCs
171 (RVOCs) and oxygenated VOCs (OVOCs). Both categories of VOCs undergo oxidation by OH,
172 resulting in the formation of RO₂, specifically RVOCRO₂ and OVOCRO₂. The interaction between
173 RVOCRO₂ and NO will produce α ANs, (1-α) NO₂, HO₂, and OVOC. Conversely, the reaction of
174 OVOCRO₂ with NO directly generates NO₂. In the Beijing-Tianjin-Hebei, Yangtze River Delta, and
175 Chengdu-Chongqing regions of China, P(HO_x) is approximately 4 ppbv/h (Lu et al., 2013; Tan et al.,
176 2018a; Tan et al., 2018b). P(HO_x) is therefore assumed to be 4 ppbv/h, with equal production rates of
177 OH and HO₂. The model also incorporates additional processes, including inter- and self-reactions of
178 RO₂, as well as reactions between NO₂ and NO, and deposition processes. In addition, during the
179 daytime, NO is determined by j(NO₂), O₃, and NO₂ according to the photo-stationary state among NO-
180 NO₂-O₃. Based on the above simplified approach, production rates of ANs and O₃ in this study can be
181 derived by direct calculations.

182 To investigate the effects of NO_x and VOCs on O₃ production, the theoretical maximum of P(O₃)
183 was simulated by a box model under varying concentrations of NO_x and VOCs. This approach was
184 employed to develop an empirical kinetic modeling approach for ozone production (EKMA). The
185 EKMA serves as a model sensitivity method to inform strategies for pollutant abatement. In this study,
186 EKMA utilizes the measured mean parameters as the initial point. Each parameter was incrementally
187 adjusted in 30 equidistant steps to create scaled arrays of VOCs and NO_x, which were subsequently
188 used to simulate the variations in P(O₃) resulting from changes in precursor concentrations. Ultimately,
189 contour plots illustrating the relationship between P(O₃) arrays versus the concentrations of NO_x and
190 VOCs are plotted based on the simulation results.

191 **3. Results and discussions**

192 **3.1 Overview of organic nitrates and precursors**

193 The duration of the Shanghai campaign was 20 days, spanning from May 25 to June 13, 2021.
194 The analysis of organic nitrates is performed from 6 a.m. to 6 p.m., as measurements taken during
195 nighttime were subject to interference from N₂O₅ and its derivatives, a phenomenon noted in previous
196 studies (Li et al., 2021; Li et al., 2023). Simultaneous measurements of PAN and PNs were conducted
197 throughout the campaign. There was a malfunction of the GC-ECD instrument from June 12 to June
198 13, during which the measurements of PAN were generally low. Relative humidity (RH) varied
199 considerably, with over 95% during rainfall periods on June 2, June 9, June 10, and June 13, while the
200 remaining days were predominantly sunny. Temperatures were high, with minimums of 20 °C and
201 daytime peaks reaching up to 36 °C. The wind speeds were generally high during the daytime and low
202 at night, with maximum of 4.2 m/s. The easterly winds prevailed during the campaign, except for May
203 27-28 and June 3-6 with mostly west and southwest winds.



204

205 **Figure 2.** The time series of the related parameters focused on organic nitrates during the campaign. The background
 206 days are represented by green B, the clean days are represented by blue C, and the ozone pollution day is represented
 207 by red P.

208 According to Chinese air quality standards for Class II areas, which define ozone pollution days
 209 as those with an hourly average exceeding 100 ppbv, the periods from May 29 to May 30 and June 5
 210 to June 6 have been identified as ozone pollution days. The remaining days were categorized as either
 211 clean or background days based on the observed daily variations in K_{OH} and CO. The daytime averages
 212 of environmental parameters during the ozone pollution period, the clean period, and the background
 213 period are presented in Table 2. Excluding cloudy and rainy days, the daytime peak of $J(O^1D)$ was
 214 near $2.8 \times 10^5 \text{ s}^{-1}$, indicating a high photochemical oxidation potential. As a secondary photochemical
 215 product, O_3 exhibited a typical daily profile, peaking at 140.5 ppbv throughout the campaign. The
 216 measurements of PNs peaked at 3.6 ppbv with a daytime average of 0.5 ± 0.3 ppbv, while ANs peaked
 217 at 1.6 ppbv with a daytime average of 0.5 ± 0.3 ppbv. Ozone pollution periods were often associated
 218 with high organic nitrates. The mean daily variation of NO_x was consistent with the characteristics of
 219 typical urban sites, significantly influenced by the morning-evening rush hours. During the daytime,
 220 NO exhibited a single peak distribution, whereas NO_2 displayed a bimodal distribution. In comparison
 221 to the background and clean period, the ozone pollution period was characterized with higher
 222 temperatures and lower humidity. Additionally, the photolysis rate and levels of $PM_{2.5}$ were both
 223 elevated during pollution days.

224 **Table 2.** Summary of daytime averages of chemical parameters over different periods during the Shanghai campaign.

Pharse	Ozone pollution	Background	Clean
T/°C	29.8±3.7	27.0±3.4	26.0±3.5



P/hPa	1043.6±0.8	1045.3±0.9	1044.3±1.4
RH/%	39.2±13.9	65.2±16.0	62.4±17.2
J(O ¹ D)×10 ⁵ /s	1.3±0.9	0.9±0.8	0.8±0.8
J(NO ₂)×10 ³ /s	4.5±2.1	2.8±2.0	2.6±1.9
NO ₂ /ppbv	17.3±6.1	16.5±5.8	20.3±7.4
NO/ppbv	3.2±2.6	4.0±2.7	4.2±3.7
O ₃ /ppbv	78.6±30.9	41.6±27.7	45.0±21.5
PM _{2.5} /μg·m ⁻³	25.9±4.3	18.3±13.4	21.9±10.0
SO ₂ /ppbv	2.2±1.7	0.4±0.5	0.6±0.7
CO/ppbv	505.3±64.3	441.6±133.3	535.0±147.8
ISO/ppbv	0.1±0.1	0.2±0.2	0.1±0.1

225

226

227

228

229

230

231

232

233

234

235

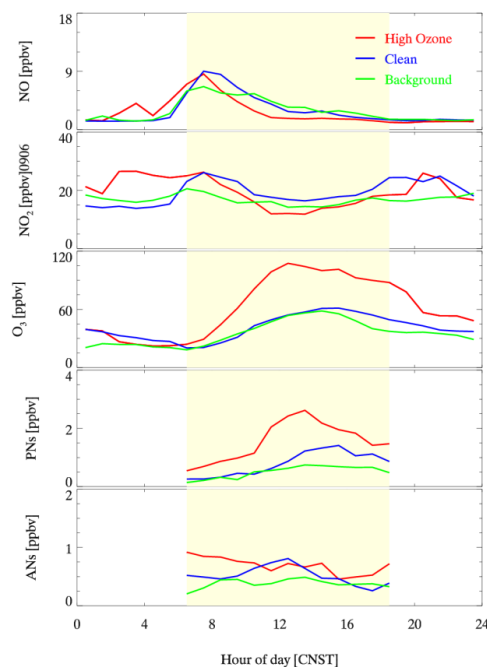
236

237

238

239

The mean diurnal profiles of organic nitrates and related parameters observed during the campaign are shown in Fig. 3. During the ozone pollution period, NO_x exhibited a peak concentration at 3:00 a.m., indicating the transport of a polluted air mass to the site. In comparison to the clean period, daytime NO_x was lower during the ozone pollution period, particularly at noon when NO dropped to as low as 1.7 ppbv. Correspondingly, ANs during the ozone pollution period were generally high, but the daily variation was not significant. Therefore, the sources of ANs were more complex during the ozone pollution period, involving both transport contribution and local production, which aligns with the significantly increased background O₃. During the clean period, the daytime peak of O₃ was notably reduced and occurred later in the day. The fluctuations in NO_x were more closely associated with morning and evening rush hours. The daytime peak of PNs decreased from 2.6 ppbv to 1.4 ppbv. In addition, the diurnal profile of ANs displayed a more pronounced peak at noon. During the background period, there was a further decline in the daytime peaks of NO_x compared to the clean period. The diurnal profile of O₃ exhibited similar trends, but the duration of high O₃ was significantly shortened. The levels of both PNs and ANs exhibited a decline, approaching the background concentrations.



240

241 **Figure 3.** Mean diurnal profiles of organic nitrates and related parameters during different observation periods.

242 Here, we compare our observations to the study previously conducted in Xinjin, which is located
243 in basin topography and faces emerging ozone pollution recently, to determine the effect of organic
244 nitrate on O₃ production under different pollution conditions (Li et al., 2023). The Shanghai and Xinjin
245 campaigns were conducted in early and late summer, respectively, exhibiting similar meteorological
246 conditions. Photochemical conditions during both two campaigns are comparable, with the daily means
247 of J(O¹D) were $0.9 \times 10^{-5} \text{ s}^{-1}$ and $0.8 \times 10^{-5} \text{ s}^{-1}$, while the daily means of J(NO₂) were $3.1 \times 10^{-3} \text{ s}^{-1}$
248 and $3.0 \times 10^{-3} \text{ s}^{-1}$, respectively, during Shanghai and Xinjin campaigns. The ratio of NO to NO₂ was 0.19
249 and 0.17 at Shanghai and Xinjin, respectively. Meanwhile, the concentration of NO_x observed in
250 Shanghai site (daily averages of 22.0 ppbv) is higher than that observed in Xinjin site (daily averages
251 of 12.5 ppbv). The concentrations of SO₂ and CO at Shanghai site were 0.9 and 491.4 ppbv, while SO₂
252 and CO were 0.6 and 404.5 ppbv, respectively. Therefore, the air masses at Shanghai site were less
253 aged than Xinjin site. However, the concentration of VOCs is lower in Shanghai campaign compared
254 to Xinjin campaign, with daily mean of 23.5 ppbv compared to 22.4 ppbv. Therefore, a comparison of
255 the two campaigns facilitates a comprehensive analysis of the impacts of organic nitrate chemistry on
256 local ozone pollution.

257 **3.2 Evaluation of organic nitrates simulations**

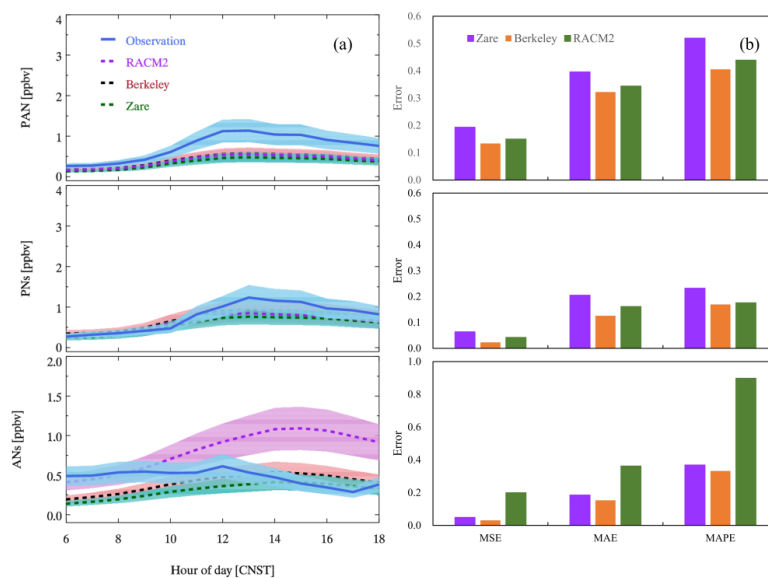
258 In light of the updates to the mechanisms, validation testing has been conducted. Our previous
259 study of the Xinjin campaign evaluated three mechanism schemes: mechanism S0, which is based on
260 RACM2, mechanism S1 and mechanism S2 which refines the budget for BVOC-derived organic



261 nitrates (Li et al., 2023). It was found that the performance of mechanism S2 for organic nitrates
262 exhibited an improvement exceeding 50%. Mechanism S2 has been updated by the Berkeley group
263 (Fisher et al., 2016; Travis et al., 2016), which includes enhancements to the production mechanism of
264 isoprene, the incorporation of the production mechanism for monoterpenes, and the completion of the
265 uptake of organic nitrates by aerosols. Additionally, the Zare mechanism further refines the production
266 mechanism of organic nitrates initiated by OH and NO₃, as well as improving the deposition process
267 of organic nitrates. As a result, the Shanghai campaign was simulated using RACM2, Berkeley, and
268 Zare mechanisms respectively for comparison.

269 The simulation result of organic nitrates under the three mechanisms is shown in Fig. 4a. The
270 simulations for PAN/PNs exhibit an overall underestimation tendency, with the simulation of PAN
271 demonstrating an even greater underestimation. Notably, the measured PNs remained above 500 pptv
272 during nighttime, indicating a continuous transportation contribution at this site. Furthermore, the
273 underestimation of PNs may be attributed to the unidentified RO_x sources. It is consistent with the
274 findings from summer campaigns in Wangdu, Beijing, where an underestimation of RO₂ was noted,
275 particularly pronounced at elevated ambient NO_x (Tan et al., 2017a). In terms of ANs, the simulation
276 performances vary across different mechanisms. A significant overestimation of ANs is evident when
277 utilized RACM2. Conversely, the simulation based on the Berkeley and Zare mechanisms generally
278 results in an underestimation of ANs, while the underestimation of the Zare mechanism is more
279 significant. Sensitivity tests conducted in Xinjin campaign suggested that the simple representation of
280 ANs uptake caused the underestimation (Li et al., 2023), which is the same reason of underestimation
281 in the Shanghai campaign. The uptake of ANs need further experimental data to achieve a detailed
282 description to support the simulations.

283 The diurnal profile of simulated PNs is consistent with the measurements, both reaching their
284 daytime peak shortly after sunrise. However, it is noteworthy that the peak concentration of PNs
285 measurements is significantly higher than the simulation. In a similar pattern with PNs, the simulated
286 ANs began to accumulate around 6:00 a.m. The measured ANs reached their peak near noon, whereas
287 the simulations peaked at 3:00 pm. To evaluate the performance of simulations, as showed in Fig. 4b,
288 three types of error ratios were calculated: Mean Square Error (MSE), Mean Absolute Error (MAE),
289 and Mean Absolute Percentage Error (MAPE). Different error metrics for the organic nitrates exhibit
290 a similar trend. The simulation performances of the Berkeley mechanism are better than the other two
291 mechanisms. As a result, the subsequent analysis is based on the Berkeley mechanism.

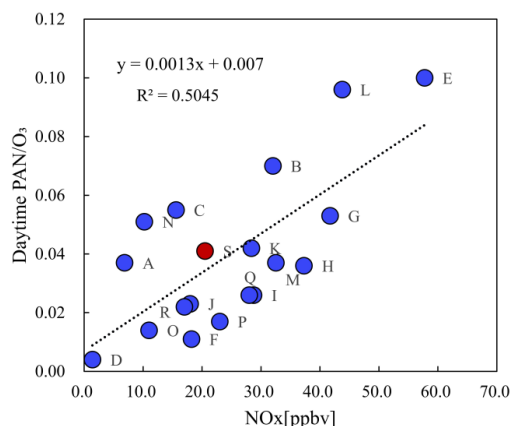


292

293 **Figure 4.** Mean diurnal profiles of observed and simulated ANs and PNs under different mechanism constraints
 294 during the Shanghai campaign (a), and the error of the different cases (b), including mean square error (MSE), mean
 295 absolute error (MAE) and mean absolute percentage error (MAPE).

296 **3.3 Impact of PNs chemistry on local ozone production**

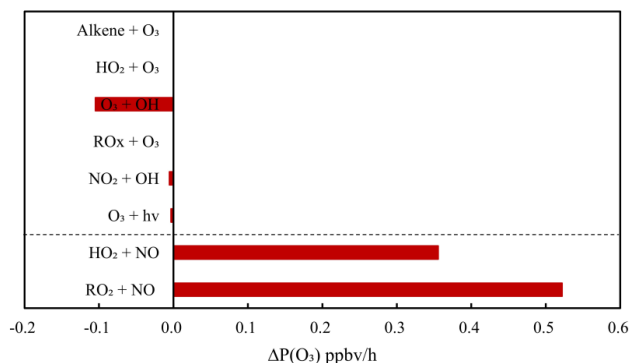
297 Organic nitrates and O₃ have common precursors, and therefore the atmospheric behavior of
 298 organic nitrates has an important influence on the local O₃ distribution. The production of PNs
 299 consumes NO₂ and RO_x, thereby directly impacting O₃ production. The relationship between the
 300 distribution of PNs and O₃ is examined throughout the campaign. Observed PAN/PNs and O₃ between
 301 9:00 a.m. and 2:00 p.m. are selected for the analysis to mitigate interference from sources that are not
 302 produced during daytime. The correlation of PAN/PNs and O₃ are shown in Fig. S1. Both PAN and
 303 PNs demonstrate a strong correlation with O₃ with the ratio of PAN/PNs to O₃ being 0.041/0.058. High
 304 ratios of PNs and O₃ usually indicate severe pollution episodes (Shepson et al., 1992; Sun et al., 2020;
 305 Zhang et al., 2023; Zhang et al., 2014). The minimum ratio of PAN/PNs and O₃ (0.024) was found
 306 during the clean periods, which can be regarded as the threshold for local photochemical pollution.
 307 NO_x is the key pollutant for production of O₃ and PNs, in order to study the relationship between the
 308 ratio of PAN/PNs to O₃ and NO_x. The daytime ratios of PAN/O₃ derived from historical field
 309 observations are summarized with corresponding NO_x concentrations in Fig. 5. The ratio derived from
 310 this study was distributed in the medium level of historical observations. The linear correlation of NO_x
 311 and PAN/O₃ ratio suggests that the NO_x concentration controls the relative production of PNs and O₃.



312

313 **Figure 5.** The relationship between historical daytime PAN/O₃ and NO_x concentrations. The red dot is the Shanghai
 314 campaign, and the blue dots are the historical campaigns. A: Grosjean et al., 2002 (Grosjean et al., 2002); B: Lee et
 315 al., 2008 (Lee et al., 2008), C: Zhang et al., 2014 (Zhang et al., 2014), D-E: Zhang et al., 2009 (Zhang et al., 2009),
 316 F-G: Zeng et al., 2019 (Zeng et al., 2019), H-K: Zhang et al., 2019 (Zhang et al., 2019), L-M: Sun et al., 2020 (Sun
 317 et al., 2020); N: Li et al., 2023 (Li et al., 2023), O-R: Xu et al., 2024 (Xu et al., 2024), S: this study.

318 Sensitivity tests were conducted based on the box model to quantify the impact of PNs
 319 photochemistry on O₃ budgets. The differences of each pathway rate are calculated at the peak of O₃
 320 production rate (Fig. 6). In the absence of PNs chemistry, two primary source pathways -namely, the
 321 reaction between RO₂ and NO, and the reaction between HO₂ and NO-exhibit large enhancements of
 322 0.52 and 0.36 ppbv/h, respectively. In comparison, O₃ sinks increase slightly in the absence of PNs
 323 photochemistry, with the reaction between OH and O₃ showing the most significant enhancement of
 324 0.11 ppbv/h. Therefore, during the Shanghai campaign, PNs photochemistry suppressed daytime ozone
 325 production mainly by reducing the reaction between HO₂ or RO₂ and NO.

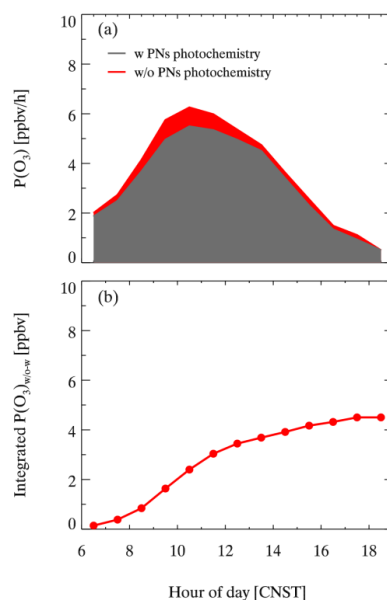


326

327 **Figure 6.** The simulated difference of ozone produce rate ($\Delta P(O_3)$) at 11am between the constraint of the PNs
 328 photochemistry and without the PNs photochemistry.



329 The PNs maintain a notable concentration until 6:00 p.m., suggesting a persistent impact on local
 330 ozone production. As shown in Fig. 7a, the PNs photochemistry began to inhibit ozone production as
 331 early as 6 a.m. and increased up to 0.8 ppbv/h (16%) at 10 a.m. The integrated inhibition of PNs
 332 photochemistry on ozone production was 4.5 ppbv during the Shanghai campaign (Fig. 7b), which was
 333 less pronounced than the Xinjin campaign. The reduced inhibition can be attributed to the lower P(PNs)
 334 observed in the Shanghai campaign (Fig. S2), where the maximum daytime PNs production rate was
 335 0.89 ppbv/h much lower than that in Xinjin campaign (3.09 ppbv/h). Therefore, the impact of PNs
 336 photochemistry on ozone production is closely linked to the PNs production, which should be
 337 elucidated through comprehensive simulation studies.



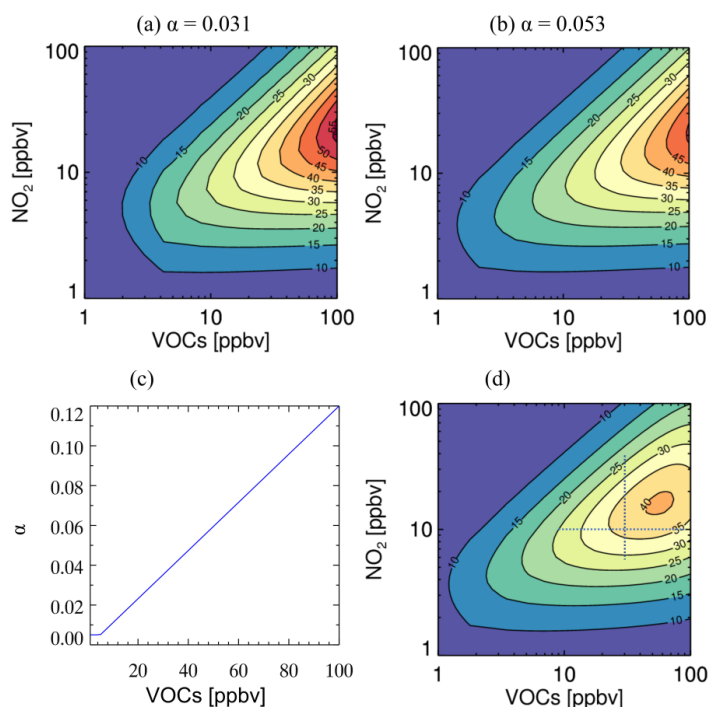
338
 339 **Figure 7.** The impact of PNs photochemistry on P(O₃) during the Shanghai campaign (a) daily changes of P(O₃)
 340 under the constraint of PNs photochemistry, (b) integrated P(O₃) change constrained by PNs photochemistry.

341 3.4 Impact of ANs chemistry on local ozone production

342 To elucidate the impact of the α on O₃ production, the EKMA was utilized to investigate the
 343 combined response of NO_x and VOCs to O₃ production at different α . The O₃ production was calculated
 344 by a simplified approach in method 2.2 and the α values were derived from weighted average of α
 345 based on the measured VOCs, the corresponding OH reaction rate constant and the α (Table S1) in
 346 Shanghai and Xinjin campaign, respectively. The model is initiated by the daytime averages of the
 347 environmental parameters. A comparative analysis is conducted between the Xinjin campaign and the
 348 Shanghai campaign where effective α is determined to be 0.031 and 0.053, respectively. As illustrated
 349 in Fig. 8a&b, P(O₃) exhibits a similar trend with the variations of NO_x and VOCs under different α ,
 350 while the value of P(O₃) reduces with larger α at the same levels of precursors. For example, when
 351 VOCs is at 8 ppbv and NO_x reaches 9 ppbv, the P(O₃) is 30.4 ppbv/h with α of 0.031, whereas it



352 decreases to 24.6 ppbv/h when α is 0.053. In addition, the larger of α in the Shanghai campaign
 353 increases the threshold of NO_x concentration for the transition of O_3 production regime. When the
 354 concentration of VOCs is fixed, a higher effective α results in a lower NO_x concentration corresponding
 355 to the peak of $\text{P}(\text{O}_3)$. Consequently, an increase in α suppresses the peak of $\text{P}(\text{O}_3)$ and simultaneously
 356 affects its sensitivity to NO_x and VOCs concentrations.



357

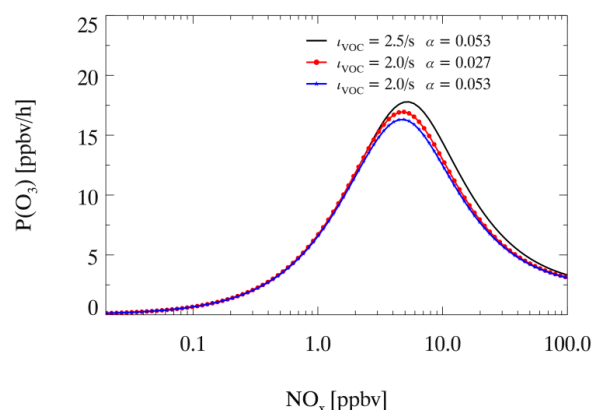
358 **Figure 8.** Ozone production ($\text{P}(\text{O}_3)$, ppb h^{-1}) derived from a simplified analytic model is plotted as a function of NO_x
 359 and VOCs under three different organic nitrate scenarios with branching ratios of (a) 0.031 for the Xinjin campaign,
 360 (b) 0.053 for the Shanghai campaign, and (d) VOC-dependent branching ratios. The branching ratio decreases from
 361 12 to 0.5% with VOC from 100 to 5 ppbv (c).

362 In the real atmosphere, the effective α of ANs tends to exhibit a decline with the reduction of
 363 VOCs concentration. Historical studies show the general range from 0.03 to 0.04 in rural sites and
 364 from 0.04 to 0.10 in urban environments, depending on the composition of VOCs and the α for BVOCs
 365 (Farmer et al., 2011; Perring et al., 2010; Perring et al., 2013; Perring et al., 2009; Rosen et al., 2004b).
 366 The clean site referenced herein was selected as the baseline, corresponding to an α value of 0.005
 367 when VOCs concentrations are less than 5 ppbv. In addition, α was set at 0.12 when the VOCs
 368 concentration was 100 ppbv. The variation of α related to VOCs concentration is shown in Fig. 8c.
 369 With a varying α , as shown in Fig. 8d, $\text{P}(\text{O}_3)$ does not follow a consistent downward trend as VOCs
 370 decrease in VOC-limited regime or transition regime. Instead, with the decrease of VOCs, the $\text{P}(\text{O}_3)$ is
 371 likely to increase at first at a relatively high VOCs distribution, and then decrease similar to the fixed
 372 α scenario. Take the cases of the horizontal dashed line as an example, at a fixed NO_x , the $\text{P}(\text{O}_3)$ start
 373 to increase as the VOCs decrease from 100 to about 60 ppbv, and subsequently decrease as VOCs



374 concentrations continue to decrease. Therefore, an increase in α directly correlates with a reduction in
 375 the $P(O_3)$ peak. As a result, a positive correlation between α and VOCs concentrations in real
 376 atmosphere might alter the NO_x -VOCs- O_3 relationship and diminish the effects of VOCs reduction on
 377 ozone control.

378 Scenarios with different VOCs reactivity and α are selected for sensitivity tests to further
 379 investigate the impact of ANs formation on the O_3 pollution control strategy in Shanghai. As illustrated
 380 in Fig. 9, variations of $P(O_3)$ among three scenarios exhibit an initial increase followed by a subsequent
 381 decrease with rising NO_x levels. For the typical VOCs reactivity and α obtained from the Shanghai
 382 campaign, the shift from NO_x -disbenefit to NO_x -limited for O_3 production occurs at a NO_x
 383 concentration of 5.4 ppbv, when $P(O_3)$ reaches a peak of 17.8 ppbv/h. When VOCs are reduced by 20%
 384 without accounting for the changes in α , the shift point for NO_x decreases to 4.9 ppbv with the $P(O_3)$
 385 peak of 16.3 ppbv/h. When the reduction of α is considered along with VOCs decrease (α decreases to
 386 0.027), the peak of $P(O_3)$ at the shift point increases by 5%. Consequently, neglecting the associated
 387 changes in α may lead to an overestimation of the effectiveness of emission control, particularly in
 388 high NO_x environments. Our observation showed that NO_x in Shanghai was notably high, which
 389 accords with the conditions in the right of the shifting point in Fig. 10. At this point, the major chain-
 390 termination reaction for the HO_x cycle is the reaction between OH and NO_2 to produce HNO_3 , while
 391 the production of ANs from the reaction between RO_2 and NO becomes relatively small. Therefore,
 392 the variation in α has a temporarily limited impact on O_3 production, whereas it should be seriously
 393 considered as NO_x levels continue to decrease.



394

395 **Figure 9.** The ozone production rate ($P(O_3)$) varies as a function of NO_x under different VOC- NO_x regimes for
 396 observed conditions in Shanghai (solid line, VOC reactivity of 2.5/s, ANs branching ratio of 0.053); a 20%
 397 reduction in VOC reactivity with a 50% reduction in branching ratio (red dot line, 2.3/s, 0.0265); a 20%
 398 reduction in VOC reactivity with no change in branching ratio (blue dot line, 2.3/s, 0.053).

399 Further comparisons of ozone production under varying precursor levels were conducted using
 400 historical observations collected in August 1994 at Mecklenburg-Vorpommern Mankmoos (MK),
 401 Germany (Ehhalt, 1999), and during the spring of 2006 in Mexico City (MX) (Farmer et al., 2011;
 402 Perring et al., 2010). The MK site serves as a typical clean background location with a very low
 403 effective α of 0.005, corresponding to τ_{VOC} of 0.4 s^{-1} , where methane is the predominant pollutant.
 404 Conversely, the MX site is characterized as an urban environment with an effective α of 0.036, where



405 a total of 58 VOCs was measured, corresponding to τ VOC of 3.1s^{-1} . The MK site shows a peak of
406 $P(\text{O}_3)$ is 2.2 ppbv/h at the NO_x of 0.63 ppbv . In contrast, the MX site demonstrates a peak $P(\text{O}_3)$ of 7.2
407 ppbv/h at a NO_x of 1.9 ppbv . Given that the Xinjin and Shanghai sites exhibit higher VOCs reactivity
408 than MX, the corresponding peak $P(\text{O}_3)$ and the NO_x inflection point are significantly elevated. This
409 increase is primarily attributed to the high $P(\text{HO}_x)$, coupled with a low α , which substantially enhances
410 $P(\text{O}_3)$ under the intensified HO_x cycling. Consequently, the ozone production potentials of urban sites
411 in China are overall higher than in other regions, while the influence of α appears to be weak.

412 4. Conclusions

413 This study reveals the abundances of PNs and ANs and quantifies their respective impacts on O_3
414 pollution based on the field campaign in Shanghai. They both showed higher values but less
415 pronounced diurnal variation during the O_3 pollution period than the clean period. The mechanism
416 validation indicates that Berkeley mechanism generally outperforms in the simulation of organic
417 nitrates. The ratio of PNs/ O_3 serves as a significant indicator of photochemistry. In comparison to the
418 previous Xinjin campaign, the inhibition effect of PNs chemistry on daytime O_3 production diminished,
419 likely attributed to the lower production of PNs. For ANs, the model simulation demonstrated that the
420 branching ratio (α) influences the NO_x -VOCs- O_3 sensitivity. The consideration of α value not only
421 alters the $P(\text{O}_3)$ peak in EKMA but also resulted in low effectiveness of precursor reductions, as the α
422 would change with the reduction of VOCs. It is worth mentioning that the complex polluted regions
423 are usually characterized by high NO_x and HO_x . In that case, the contribution of chain-termination
424 reactions that produce ANs could be reduced, leading to limited impact of AN chemistry on O_3
425 formation. The effect of ANs chemistry on O_3 pollution control is therefore expected to enhance with
426 further precursor reductions, and we suggest a pressing need for more measurements and analysis of
427 organic nitrates to address the forthcoming challenges in air pollution mitigation.

428

429 **Code/Data availability.** The datasets used in this study are available from the corresponding author
430 upon request (chenxr95@mail.sysu.edu.cn; k.lu@pku.edu.cn).

431

432 **Author contributions.** K.D.L. and X.R.C. designed the study. C.M.L. and X.R.C. analyzed the data
433 and wrote the paper with input from K.D.L.

434

435 **Competing interests.** The authors declare that they have no conflicts of interest.

436

437 **Acknowledgments.** This work was supported by the National Natural Science Foundation of China
438 (Grants No. 42407139); the National Natural Science Foundation of China (Grants No. 22406204);
439 the special fund of State Environmental Protection Key Laboratory of Formation and Prevention of
440 Urban Air Pollution Complex (SEPAir-2024080219); the Innovative Exploration Program of National
441 Institute of Metrology, China (No. AKYCX2313).

442



443 **References**

- 444 Arey J, Aschmann SM, Kwok ESC, Atkinson R. Alkyl Nitrate, Hydroxyalkyl Nitrate, and Hydroxycarbonyl Formation
445 from the NO_x-Air Photooxidations of C₅-C₈ n-Alkanes. *The Journal of Physical Chemistry A* 2001; 105: 1020-
446 1027.
- 447 Aruffo E, Di Carlo P, Dari-Salisburgo C, Biancofiore F, Giammaria F, Busilacchio M, et al. Aircraft observations of the
448 lower troposphere above a megacity: Alkyl nitrate and ozone chemistry. *Atmospheric Environment* 2014; 94: 479-
449 488.
- 450 Ashmore MR. Assessing the future global impacts of ozone on vegetation. *Plant Cell and Environment* 2005; 28: 949-964.
- 451 Browne EC, Cohen RC, Wooldridge PJ, Valin LC, Min K-E. Organic nitrate formation: Impacts on NO_x lifetime and ozone.
452 *Abstracts of Papers of the American Chemical Society* 2012; 244.
- 453 Browne EC, Min KE, Wooldridge PJ, Apel E, Blake DR, Brune WH, et al. Observations of total RONO₂ over the boreal
454 forest: NO_x sinks and HNO₃ sources. *Atmospheric Chemistry and Physics* 2013; 13: 4543-4562.
- 455 Chen J, Wu H, Liu AW, Hu SM, Zhang J. Field Measurement of NO₂ and RNO₂ by Two-Channel Thermal Dissociation
456 Cavity Ring Down Spectrometer. *Chinese Journal of Chemical Physics* 2017; 30: 493-498.
- 457 Darer AI, Cole-Filipiak NC, O'Connor AE, Elrod MJ. Formation and Stability of Atmospherically Relevant Isoprene-
458 Derived Organosulfates and Organonitrates. *Environmental Science & Technology* 2011; 45: 1895-1902.
- 459 Day DA, Dillon MB, Wooldridge PJ, Thornton JA, Rosen RS, Wood EC, et al. On alkyl nitrates, O₃, and the "missing
460 NO_y". *Journal of Geophysical Research-Atmospheres* 2003; 108.
- 461 Ehhalt DH. Photooxidation of trace gases in the troposphere. *Physical Chemistry Chemical Physics* 1999; 1: 5401-5408.
- 462 Farmer DK, Perring AE, Wooldridge PJ, Blake DR, Baker A, Meinardi S, et al. Impact of organic nitrates on urban ozone
463 production. *Atmospheric Chemistry and Physics* 2011; 11: 4085-4094.
- 464 Fisher JA, Jacob DJ, Travis KR, Kim PS, Marais EA, Miller CC, et al. Organic nitrate chemistry and its implications for
465 nitrogen budgets in an isoprene- and monoterpene-rich atmosphere: constraints from aircraft (SEAC(4)RS) and
466 ground-based (SOAS) observations in the Southeast US. *Atmospheric Chemistry and Physics* 2016; 16: 5969-5991.
- 467 Flocke F, Volz-Thomas A, Buers HJ, Patz W, Garthe HJ, Kley D. Long-term measurements of alkyl nitrates in southern
468 Germany I. General behavior and seasonal and diurnal variation. *Journal of Geophysical Research-Atmospheres* 1998;
469 103: 5729-5746.
- 470 Gao W, Tie X, Xu J, Huang R, Mao X, Zhou G, et al. Long-term trend of O₃ in a mega City (Shanghai), China:
471 Characteristics, causes, and interactions with precursors. *Science of the Total Environment* 2017; 603: 425-433.
- 472 Grosjean E, Grosjean D, Woodhouse LF, Yang YJ. Peroxyacetyl nitrate and peroxypropionyl nitrate in Porto Alegre, Brazil.
473 *Atmospheric Environment* 2002; 36: 2405-2419.
- 474 Ito A, Sillman S, Penner JE. Global chemical transport model study of ozone response to changes in chemical kinetics and
475 biogenic volatile organic compounds emissions due to increasing temperatures: Sensitivities to isoprene nitrate
476 chemistry and grid resolution. *Journal of Geophysical Research-Atmospheres* 2009; 114.
- 477 Lee G, Jang Y, Lee H, Han J-S, Kim K-R, Lee M. Characteristic behavior of peroxyacetyl nitrate (PAN) in Seoul megacity,
478 Korea. *Chemosphere* 2008; 73: 619-628.
- 479 Li C, Wang H, Chen X, Zhai T, Chen S, Li X, et al. Thermal dissociation cavity-enhanced absorption spectrometer for
480 measuring NO₂, RO₂NO₂, and RONO₂ in the atmosphere. *Atmospheric Measurement Techniques* 2021; 14: 4033-
481 4051.
- 482 Li C, Wang H, Chen X, Zhai T, Ma X, Yang X, et al. Observation and modeling of organic nitrates on a suburban site in
483 southwest China. *Science of the Total Environment* 2023; 859.
- 484 Liebmann J, Karu E, Sobanski N, Schuladen J, Ehn M, Schallhart S, et al. Direct measurement of NO₃ radical reactivity
485 in a boreal forest. *Atmospheric Chemistry and Physics* 2018; 18: 3799-3815.
- 486 Liebmann J, Sobanski N, Schuladen J, Karu E, Hellen H, Hakola H, et al. Alkyl nitrates in the boreal forest: formation via
487 the NO₃-, OH- and O₃-induced oxidation of biogenic volatile organic compounds and ambient lifetimes.
488 *Atmospheric Chemistry and Physics* 2019; 19: 10391-10403.
- 489 Ling ZH, Guo H, Simpson IJ, Saunders SM, Lam SHM, Lyu XP, et al. New insight into the spatiotemporal variability and
490 source apportionments of C-1-C-4 alkyl nitrates in Hong Kong. *Atmospheric Chemistry and Physics* 2016; 16: 8141-
491 8156.
- 492 Liu Y, Shen H, Mu J, Li H, Chen T, Yang J, et al. Formation of peroxyacetyl nitrate (PAN) and its impact on ozone
493 production in the coastal atmosphere of Qingdao, North China. *Science of the Total Environment* 2021; 778.
- 494 Lu KD, Hofzumahaus A, Holland F, Bohn B, Brauers T, Fuchs H, et al. Missing OH source in a suburban environment near
495 Beijing: observed and modelled OH and HO₂; concentrations in summer 2006. *Atmospheric
496 Chemistry and Physics* 2013; 13: 1057-1080.
- 497 Monks PS, Archibald AT, Colette A, Cooper O, Coyle M, Derwent R, et al. Tropospheric ozone and its precursors from the
498 urban to the global scale from air quality to short-lived climate forcer. *Atmos. Chem. Phys.* 2015; 15: 8889-8973.
- 499 Ng NL, Brown SS, Archibald AT, Atlas E, Cohen RC, Crowley JN, et al. Nitrate radicals and biogenic volatile organic



500 compounds: oxidation, mechanisms, and organic aerosol. *Atmospheric Chemistry and Physics* 2017; 17: 2103-2162.
501 Perring AE, Bertram TH, Farmer DK, Wooldridge PJ, Dibb J, Blake NJ, et al. The production and persistence of Sigma
502 RONO₂ in the Mexico City plume. *Atmospheric Chemistry and Physics* 2010; 10: 7215-7229.
503 Perring AE, Pusede SE, Cohen RC. An Observational Perspective on the Atmospheric Impacts of Alkyl and Multifunctional
504 Nitrates on Ozone and Secondary Organic Aerosol. *Chemical Reviews* 2013; 113: 5848-5870.
505 Perring AE, Wisthaler A, Graus M, Wooldridge PJ, Lockwood AL, Mielke LH, et al. A product study of the isoprene+NO₃
506 reaction. *Atmospheric Chemistry and Physics* 2009; 9: 4945-4956.
507 Present PSR, Zare A, Cohen RC. The changing role of organic nitrates in the removal and transport of NO_x. *Atmospheric*
508 *Chemistry and Physics* 2020; 20: 267-279.
509 Reisen F, Aschmann SM, Atkinson R, Arey J. 1,4-hydroxycarbonyl products of the OH radical initiated reactions of C-5-
510 C-8 n-alkanes in the presence of NO. *Environmental Science & Technology* 2005; 39: 4447-4453.
511 Roberts JM, Bertman SB. The thermal-decomposition of peroxyacetic nitric anhydride (pan) and peroxyacetic nitric
512 anhydride (MPAN). *International Journal of Chemical Kinetics* 1992; 24: 297-307.
513 Romer PS, Duffey KC, Wooldridge PJ, Allen HM, Ayres BR, Brown SS, et al. The lifetime of nitrogen oxides in an
514 isoprene-dominated forest. *Atmospheric Chemistry and Physics* 2016; 16: 7623-7637.
515 Romer PS, Duffey KC, Wooldridge PJ, Edgerton E, Baumann K, Feiner PA, et al. Effects of temperature-dependent NO_x
516 emissions on continental ozone production. *Atmospheric Chemistry and Physics* 2018; 18: 2601-2614.
517 Rosen RS, Wood EC, Wooldridge PJ, Thornton JA, Day DA, Kuster W, et al. Observations of total alkyl nitrates during
518 Texas Air Quality Study 2000: Implications for O₃ and alkyl nitrate photochemistry. *Journal of Geophysical*
519 *Research-Atmospheres* 2004a; 109: 15.
520 Rosen RS, Wood EC, Wooldridge PJ, Thornton JA, Day DA, Kuster W, et al. Observations of total alkyl nitrates during
521 Texas Air Quality Study 2000: Implications for O₃ and alkyl nitrate photochemistry. *Journal of Geophysical*
522 *Research-Atmospheres* 2004b; 109.
523 Sadanaga Y, Takaji R, Ishiyama A, Nakajima K, Matsuki A, Bandow H. Thermal dissociation cavity attenuated phase shift
524 spectroscopy for continuous measurement of total peroxy and organic nitrates in the clean atmosphere. *Review of*
525 *Scientific Instruments* 2016; 87.
526 Schwantes RH, Emmons LK, Orlando JJ, Barth MC, Tyndall GS, Hall SR, et al. Comprehensive isoprene and terpene gas-
527 phase chemistry improves simulated surface ozone in the southeastern US. *Atmospheric Chemistry and Physics* 2020;
528 20: 3739-3776.
529 Shepson PB, Hastie DR, So KW, Schiff HI. Relationships between PAN, PPN and O₃ at urban and rural sites in Ontario.
530 *Atmospheric Environment Part a-General Topics* 1992; 26: 1259-1270.
531 Song J, Zhang Y, Huang Y, Ho KF, Yuan Z, Ling Z, et al. Seasonal variations of C-1-C-4 alkyl nitrates at a coastal site in
532 Hong Kong: Influence of photochemical formation and oceanic emissions. *Chemosphere* 2018; 194: 275-284.
533 Sun J, Li Z, Xue L, Wang T, Wang X, Gao J, et al. Summertime C-1-C-5 alkyl nitrates over Beijing, northern China: Spatial
534 distribution, regional transport, and formation mechanisms. *Atmospheric Research* 2018; 204: 102-109.
535 Sun M, Cui Jn, Zhao X, Zhang J. Impacts of precursors on peroxyacetyl nitrate (PAN) and relative formation of PAN to
536 ozone in a southwestern megacity of China. *Atmospheric Environment* 2020; 231.
537 Tan Z, Fuchs H, Lu K, Hofzumahaus A, Bohn B, Broch S, et al. Radical chemistry at a rural site (Wangdu) in the North
538 China Plain: observation and model calculations of OH, HO₂ and RO₂ radicals. *Atmos. Chem. Phys.* 2017a; 17: 663-
539 690.
540 Tan Z, Fuchs H, Lu K, Hofzumahaus A, Bohn B, Broch S, et al. Radical chemistry at a rural site (Wangdu) in the North
541 China Plain: observation and model calculations of OH, HO₂ and RO₂ radicals. *Atmospheric Chemistry and Physics* 2017b; 17: 663-690.
542 RO₂ radicals. *Atmospheric Chemistry and Physics* 2017b; 17: 663-690.
543 Tan Z, Lu K, Jiang M, Su R, Dong H, Zeng L, et al. Exploring ozone pollution in Chengdu, southwestern China: A case
544 study from radical chemistry to O₃-VOC-NO_x sensitivity. *Sci Total Environ* 2018a; 636: 775-786.
545 Tan ZF, Rohrer F, Lu KD, Ma XF, Bohn B, Broch S, et al. Wintertime photochemistry in Beijing: observations of RO_x
546 radical concentrations in the North China Plain during the BEST-ONE campaign. *Atmospheric Chemistry and Physics*
547 2018b; 18: 12391-12411.
548 Teng AP, Crouse JD, Lee L, St Clair JM, Cohen RC, Wennberg PO. Hydroxy nitrate production in the OH-initiated
549 oxidation of alkenes. *Atmospheric Chemistry and Physics* 2015; 15: 4297-4316.
550 Travis KR, Jacob DJ, Fisher JA, Kim PS, Marais EA, Zhu L, et al. Why do models overestimate surface ozone in the
551 Southeast United States? *Atmospheric Chemistry and Physics* 2016; 16: 13561-13577.
552 Wang M, Shao M, Chen W, Lu S, Wang C, Huang D, et al. Measurements of C1-C4 alkyl nitrates and their relationships
553 with carbonyl compounds and O₃ in Chinese cities. *Atmospheric Environment* 2013; 81: 389-398.
554 Wang W, Parrish DD, Wang S, Bao F, Ni R, Li X, et al. Long-term trend of ozone pollution in China during 2014-2020:
555 distinct seasonal and spatial characteristics and ozone sensitivity. *Atmospheric Chemistry and Physics* 2022; 22: 8935-
556 8949.



- 557 Xu T, Nie W, Xu Z, Yan C, Liu Y, Zha Q, et al. Investigation on the budget of peroxyacetyl nitrate (PAN) in the Yangtze
558 River Delta: Unravelling local photochemistry and regional impact. *Science of the Total Environment* 2024; 917.
- 559 Xue K, Zhang X. The rationale behind updates to ambient ozone guidelines and standards. *Frontiers in Public Health* 2023;
560 11.
- 561 Yeh GK, Ziemann PJ. Alkyl Nitrate Formation from the Reactions of C_8-C_{14} -Alkanes
562 with OH Radicals in the Presence of NO_x : Measured Yields with Essential Corrections for Gas-
563 Wall Partitioning. *Journal of Physical Chemistry A* 2014a; 118: 8147-8157.
- 564 Yeh GK, Ziemann PJ. Identification and Yields of 1,4-Hydroxynitrates Formed from the Reactions of C_8-C_{16} -
565 Alkanes with OH Radicals in the Presence of NO_x . *Journal of
566 Physical Chemistry A* 2014b; 118: 8797-8806.
- 567 Young PJ, Naik V, Fiore AM, Gaudel A, Guo J, Lin MY, et al. Tropospheric Ozone Assessment Report: Assessment of
568 global-scale model performance for global and regional ozone distributions, variability, and trends. *Elementa-Science
569 of the Anthropocene* 2018; 6.
- 570 Zare A, Romer PS, Tran N, Keutsch FN, Skog K, Cohen RC. A comprehensive organic nitrate chemistry: insights into the
571 lifetime of atmospheric organic nitrates. *Atmospheric Chemistry and Physics* 2018; 18: 15419-15436.
- 572 Zeng L, Fan G-J, Lyu X, Guo H, Wang J-L, Yao D. Atmospheric fate of peroxyacetyl nitrate in suburban Hong Kong and
573 its impact on local ozone pollution. *Environmental Pollution* 2019; 252: 1910-1919.
- 574 Zhang B, Zhao X, Zhang J. Characteristics of peroxyacetyl nitrate pollution during a 2015 winter haze episode in Beijing.
575 *Environmental Pollution* 2019; 244: 379-387.
- 576 Zhang G, Xia L, Zang K, Xu W, Zhang F, Liang L, et al. The abundance and inter-relationship of atmospheric peroxyacetyl
577 nitrate (PAN), peroxypropionyl nitrate (PPN), O-3, and NO_y during the wintertime in Beijing, China. *Science of the
578 Total Environment* 2020; 718.
- 579 Zhang H, Tong S, Zhang W, Xu Y, Zhai M, Guo Y, et al. A comprehensive observation on the pollution characteristics of
580 peroxyacetyl nitrate (PAN) in Beijing, China. *Science of the Total Environment* 2023; 905.
- 581 Zhang H, Xu X, Lin W, Wang Y. Wintertime peroxyacetyl nitrate (PAN) in the megacity Beijing: Role of photochemical
582 and meteorological processes. *Journal of Environmental Sciences* 2014; 26: 83-96.
- 583 Zhang JM, Wang T, Ding AJ, Zhou XH, Xue LK, Poon CN, et al. Continuous measurement of peroxyacetyl nitrate (PAN)
584 in suburban and remote areas of western China. *Atmospheric Environment* 2009; 43: 228-237.
- 585 Zhu W, Zhou M, Cheng Z, Yan N, Huang C, Qiao L, et al. Seasonal variation of aerosol compositions in Shanghai, China:
586 Insights from particle aerosol mass spectrometer observations. *Science of The Total Environment* 2021; 771: 144948.
587